Reconstructing Human Joint Motion with Computational Fabrics

ANONYMOUS AUTHOR(S)

Accurate and continuous monitoring of joint rotational motion is crucial for a wide range of applications such as physical rehabilitation and motion training. Existing motion capture systems, however, either need heavy instrumentation in the environment, or fail to track arbitrary joint motion, or impose wearing discomfort by requiring rigid electrical sensors right around the joint area. This work studies the use of everyday fabrics as a flexible and soft sensing medium to monitor joint angular motion accurately and reliably. Specifically we focus on the primary use of conductive stretchable fabrics to sense the skin deformation during joint motion and infer the joint rotational angle. We tackle challenges of fabric sensing originated by the inherent properties of elastic materials by leveraging two types of sensing fabric and characterizing their properties based on models in material science. We apply models from bio-mechanics to infer joint angles and propose the use of dual strain sensing to enhance sensing robustness against user diversity and fabric position offsets. We fabricate prototypes using off-the-shelf fabrics and micro-controller. Experiments with ten participants show 9.69° mean angular error in tracking joint angle and its sensing robustness across various users and activities.

CCS Concepts: • **Human-centered computing → Ubiquitous and mobile computing systems and tools**; **Ambient intelligence**;

Additional Key Words and Phrases: smart fabric/textile, fabric/textile sensing, joint motion sensing

ACM Reference Format:
Anonymous Author(s). 2018. Reconstructing Human Joint Motion with Computational Fabrics. *Proc. ACM Interact. Mob. Wearable Ubiquitous Technol.* 0, 0, Article 0 (2018), 25 pages.

1 INTRODUCTION

Human body joints are essential for actuating body motion. Accurate and continuous monitoring of their rotational movement is critical for physical rehabilitation, motion training/coaching, sports analytics, human-robot or human-computer interactions. For rehabilitation patients with joint injuries or chronic joint pains, day-to-day measurement of joint's angular motion helps doctors assess the effectiveness of medical and physical treatments, since joint and muscle repair takes long enough that it is impractical for expert therapists to remain with patients at all times; for students learning precise motions from instructors in the educational context (e.g., athletic coaching, yoga training, learning to perform a complex surgical procedure), monitoring joint angles allows instructors to analyze detailed joint movements and provide fine-grained corrections and feedback.

All these applications demand joint motion sensing systems that are portable, comfortable for long-time wear, and capable of sensing subtle motion. Existing technologies on motion capture, however, still fall short in meeting these requirements. High-end systems such as VICON [87] or Kinect require heavy instrumentation of the environment (e.g., setting up multiple infrared cameras). More portable systems either achieve coarse sensing granularity by classifying a limited set of gestures/poses and thus cannot track arbitrary motion, or require users to constantly wear rigid electrical sensors right around the joint area [22, 74, 91], where such placement inflexibility often causes the system burdensome to wear.

2474-9567/2018/0-ART0 $15.00
https://doi.org/

In this work we consider the use of everyday fabrics as an unobtrusive sensing medium to continuously and accurately monitor joint angular motion. Requiring neither infrastructure support nor rigid electrical sensors on the joint, our approach relies on fabrics/textile *alone*, as a soft and natural sensing layer around joints, to reconstruct the angles of body joints at a fine granularity. While the concept of e-textile has been proposed in prior studies for various applications, prior works either offer coarse sensing capabilities [50, 58, 62, 81] or still require embedding electronics into textiles by using textile as a substrate for attachment of sensors. We aim to advance the state-of-the-art by achieving qualitative advances in sensing capability and reliability, and more importantly, by focusing on the use of off-the-shelf, low-cost (e.g., $50) fabrics alone for motion sensing without extra electrical sensors. Such a minimalist sensing approach renders the sensing system comfortable to wear, low-power, and low-cost.

Specifically, we study primarily the use of conductive stretchable fabrics with knitted structures. As shown in Figure 2(b), a knitted fabric is constructed by a continuous loop of yarns. Made of conductive stretchable threads, the knitted fabric reacts to different levels of strain with varying resistance. The change in resistance is caused by alterations of yarns' contact points and contact pressure under the tension [34]. This property can be exploited to sense body joint motion, where we wrap a joint with conductive stretchable fabrics (also serving as a joint protective wrap commonly worn during exercises for joint protection). Joint rotation and muscle movement cause skin deformation and thus strain of the fabric. By continuously monitoring the fabric's resistance, we can infer the muscle strain caused by the current joint motion, and thus recover the joint angle. The system only requires a micro-controller fetching data on fabric resistance through conductive threads. The micro-controller can be placed away from the joint with great flexibility for the comfort of wear. As an example, it can be embedded into a button to hide its appearance and it can be easily detached when necessary.

To realize this conceptually simple idea as a practical system providing accurate and robust motion sensing, we are confronted with several challenges. *First*, with off-the-shelf stretchable fabrics, the resistance change and the level of strain do not exhibit an one-to-one mapping, and even worse, their relationship depends on the type of motion (e.g., flexion/loading or extension/unloading), caused by the *hysteresis* intrinsic to elastic materials. It results into ambiguities in inferring skin deformation solely based on the observed changes in fabric resistance. *Second*, fabric as a strain sensor does not provide a stable output even under a constant strain. This is a phenomenon common in stretchable materials and referred to as the *stress relaxation* in material science. Such relaxation further increases the ambiguity in inferring skin deformation and leads to errors that accumulate over time. *Third*, even with perfect derivation of skin deformation, inferring the actual joint angle is still nontrivial. For one, bone shape and soft tissue distribution differ significantly across users. Additionally, joint motion can lead to subtle slide of the sensing fabrics around the joint. Both individual differences and the motion artifact of the sensing fabrics pose challenges in achieving robust motion sensing in practice.

We address above challenges as follows. To disambiguate motion states, we add a small piece of pressure fabric to augment the primary sensing fabric (i.e., strain sensors). Pressure fabric senses the pressure from the joint to the fabric during motions. Although it alone cannot provide precise sensing of subtle motion, it can steadily differentiate coarse motion states: flexion, extension, or the motionless state. We characterize strain fabric's resistance change in different motion states, and apply models from material sciences to compensate for the stress relaxation during the motionless state. Finally, we leverage models in the literature of bio-mechanics to characterize the geometric relationship between skin deformation and joint angle. To deal with individual differences and motion artifact of the sensing fabrics, we place two straps of strain fabrics as dual sensors above the joint. We consider the differences of the stretch lengths of these two strain fabrics, which cancel out the impact of the body part thickness or slight offset of fabric positions.

With the elbow joint as an example, we fabricate prototypes in two sizes (27cm/20.5cm lower-elbow diameter, 31cm/23cm upper-elbow diameter) using off-the-shelf fabrics and micro-controller (Adafruit Flora). We place strain fabrics and pressure fabrics in separate layers to enhance their sensing resilience and sensitivity. Inelastic

fabrics are used as reference resistor for the micro-controller to monitor the resistance change of strain and pressure fabrics, where micro-controller and sensing fabrics are connected via conductive threads. we test our prototypes with ten participants to examine sensing accuracy and robustness. We also seek participants' feedback on the wearing comfort.

2 BACKGROUND ON FABRIC SENSING

Fabric as a sensor presents numerous benefits, as it is soft, light, flexible, and thus easy to wear even during exercises. In particular, our study considers off-the-shelf stretchable textile made of conductive threads as our primary sensing fabric. The sensing ability of such fabrics stems from their knitted micro-structures of the yarns, where an external strain causes changes in the number of contact points and contact pressure, resulting into changes in the contact resistance of the fabric [16, 34, 64, 79]. We next experimentally examine the property of such fabrics and their sensing capability.

Experimental Validation. We test an off-the-shelf stretchable conductive fabric (LessEMF #A321) [37]. With 76% Nylon and 24% elastic fiber, it can be stretched by up to 100% along its length/course direction and 60% along its width/wale direction. Its yearns are plated with a thin silver layer offering great conductivity. We cascade the test fabric with a fixed-value reference resistance. We use a micro-controller to measure the voltage on the test fabric to monitor its resistance change under various levels of strain. To systematically apply various levels of strain, we use a professional tensile test machine (Instron 4442). Figure 1 illustrates the overall setup. We evaluate fabric's resistance change via the metric of *resistance change ratio* $r_{\Delta R} = (R_2 - R_1)/R_1$, where R_1 and R_2 denote the original and current resistance, respectively. With the original voltage as U_1 and current voltage as U_2, $r_{\Delta R}$ can be computed as:

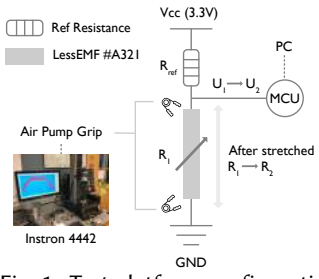

Fig. 1. Test platform configuration

$$r_{\Delta R} = \frac{R_2 - R_1}{R_1} = \frac{V_{cc}U_2 - U_1U_2}{V_{cc}U_1 - U_1U_2} - 1, \tag{1}$$

where V_{cc} is the power supply voltage from the micro-controller.

Figure 2(a) plots the resistance change ratio as a 15 cm × 3 cm fabric is stretched along its course direction. We also plot the stress on the fabric recored by Instron. We obtain two main observations. *First*, the fabric is very sensitive to motion, where even millimeter-level stretches cause noticeable changes in resistance (e.g., 2cm stretch leads to 60% resistance change). It provides basis for sensing fine-grained motion. *Second*, as the strain grows, the change in fabric resistance is not monotonic; rather, it undergoes a sharp increase, followed by a gradual decline. We observe similar patterns consistently across various test runs and across other types of stretchable fabrics we have tested. This pattern can be explained by examining how contact points and contact pressure are altered under strain. Based on the Holm's theory [34], the contact resistance of a conductive fabric is inversely proportional to the number of contact points and the contact pressure. In the beginning when the fabric is being slightly stretched, the stress on the fabric is not evident and the change in the number of contact points dominates the resistance change. The low level of strain only causes fiber slipping within air gaps and forming tighter block structure. As a result, the number of contact points decreases, leading to an increase in contact resistance. As the fabric is further stretched under higher levels of strain, the stress on the fabric becomes the dominant factor that changes the resistance. Since there is no more space for yarns to form blocks, the number of contact points stays constant. The growing inner stress among yarns leads to the decline of the contact resistance. Figure 2(b) illustrates fabric's micro-structure during different phases of the process.

We further test the resistance change as we stretch the fabric in the wale direction. We cut two pieces of fabrics in the same size (15cm × 3cm), one with course direction along its length and the other with wale direction along

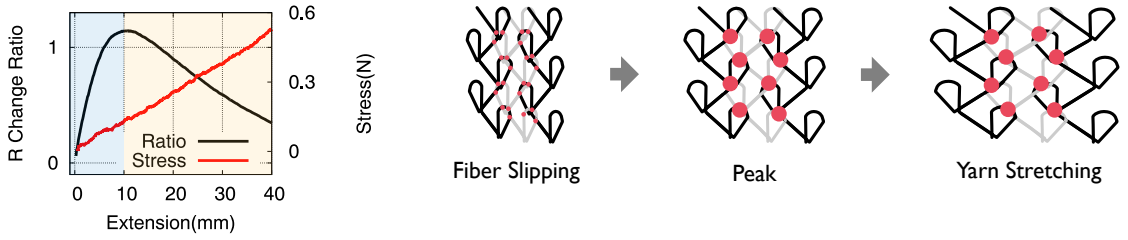

(a) Overall trend (b) Various phases during a stretch

Fig. 2. The change of fabric resistance as the fabric is stretched. Resistance sharply increases due to the decrease in yarn contact points during fiber slipping, and then gradually decreases under increasing contact pressure during yarn stretching.

its length. We stretch both fabrics to 30% of its original length and plot the resistance change ratios in Figure 3(a). We observe that resistance change exhibits a similar trend yet with distinct details: stretch in the course direction leads to much more significant changes in resistance (over 100%), while that in the wale direction leads to only around 5% change in the resistance. Figure 3(b) and 3(c) show the microscope images of each fabric under 30% strain.

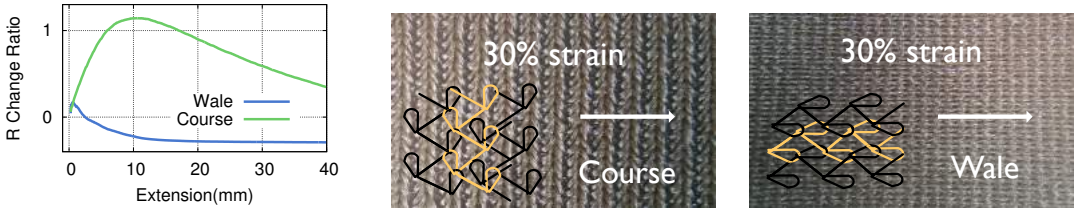

(a) Impact of stretch direction (b) 30% strain in the course direction (c) 30% strain in the wale direction

Fig. 3. Resistance change of stretchable conductive fabric when it is stretched along its wale or course direction (a). (b) and (c) are microscope images on fabric's micro-structure under 30% strain along the course and wale direction, respectively.

We also examine the impact of fabric's size ratio on its sensitivity to strain. Figure 4 compares various fabrics in various size configurations when they are stretched in the course direction. We observe that increases in the width result into higher peaks, because more yarn blocks are formed, leading to fewer contact points and larger increase in resistance. On the other hand, under a fixed width, longer fabrics have more air gaps in the stretching direction and thus need more strain to reach the peak, leading to the peak occurred under larger stretch lengths. Additionally, we observe that a thinner fabric (1-cm width) has more high-frequency noise in its signal response. We hypothesize that the thinner fabric has weaker fiber strength, making it harder to keep a stable structure and stable resistance value. Overall, wider and longer fabrics are more preferable for sensing purposes.

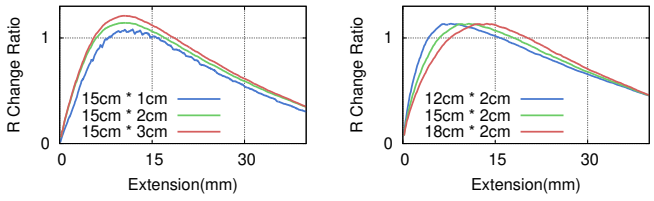

(a) Varying width (b) Varying length

Fig. 4. Impact of fabric size configuration on its sensitivity to stretch.

Summary. Our experiments results validate that off-the-shelf stretchable conductive fabrics are sensitive to motion when they are stretched along the course direction. Even millimeter-level stretches lead to noticeable changes in resistance, providing basis for the fabric to sense skin deformation caused by subtle joint motion. Under

increasing strain, the change in fabric's resistance is non-monotonic, starting with a sharp increase followed by a gradual decline. Wider and longer fabrics provide more stable, substantial change in resistance under strain.

3 CHALLENGES IN FABRIC SENSING

While prior results are promising, fabric as a sensor also presents numerous challenges, especially for the purpose of accurately and robustly inferring joint angles. We elaborate on the challenges as follows.

Elastic Hysteresis. The non-monotonic nature of the fabric resistance change under increasing strain indicates that there is no one-to-one mapping between the observed resistance change and the stretch length. Compounding this problem is the fact that the characterization of the resistance change also depends on the type of motion. When the fabric is being extended under strain (loading), its resistance change follows a curve that is different from that when the fabric is retracting as the strain is reduced (unloading). The difference is due to the energy dissipation caused by material internal friction. This phenomenon is referred to as *hysteresis*, an intrinsic property of elastic materials. As an example, Figure 5 plots the ratio of resistance change during loading and unloading, with the LessEMF fabric (15.3cm × 3cm in size). It implies that an observed value of resistance change can correspond to up to four possible stretch lengths, making it hard to uniquely infer the current skin deformation.

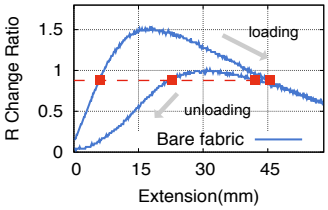

Fig. 5. Elastic hysteresis. Resistance change follows a different curve during loading/extending and unloading/retracting.

Instability. Furthermore, our experiments reveal that the impact of strain on fabric's resistance change slightly varies across repeated rounds of stretching. Thus, it is difficult to characterize the mapping between resistance change and extension length using a single function with fixed parameters. To examine this instability, we stretch a 15 cm × 1.5 cm fabric to 30% of its original length along the wale direction and repeat it for 160 rounds. Figure 6(a) plots the resistance change ratio as the extension length increases. We observe that curves from different rounds do not exactly overlap and exhibit slight offsets. As suggested in [40], a dominant factor causing these offsets is the electromagnetic noise from the environment. Here each conductive thread of the fabric can be seen as an antenna and the large number of threads can easily absorb electromagnetic noise from the environment, affecting how fabric's resistance changes under strain.

Stress Relaxation. Another challenge comes from the fact that fabric resistance does not stay at a stable value under a constant strain. This is known as *stress relaxation* in the literature of material science, a property commonly seen in elastic polymer because of the loose connection of its fiber [42, 73]. Figure 6(b) plots the resistance change ratio as a LessEMF fabric (15 cm × 1.5 cm in size) is stretched three times by the Instron tensile machine, where each time the strain is kept constant for 60 seconds. We observe that the resistance slowly drops by 12% after 5 seconds under a constant strain. Such instability brings more ambiguities in deriving a single deformation/stretch value based on the observed resistance change.

User Diversity and Motion Artifact. Finally, inferring the actual joint angle based on the sensed deformation on the skin is challenging given the differences of body parameters and motion patterns across users. This has been confirmed as one of the main sources of error in designing wearable systems in prior works [19, 32]. Specifically in our context, the relationship between the joint angle and the skin surface deformation depends on the bone shape and soft tissue distribution. Additionally, sensing fabrics can slightly slide during joint motions. As a result, the stretchable fabric can end up measuring skin deformation at various spots during the course of a motion, and the measurement inconsistency can hurt sensing accuracy. To address such motion artifact, prior works have considered applying a calibration in the beginning of each wearing [21, 23, 27, 44, 77], or the use of sensor array with machine learning algorithms [18, 33, 50, 53]. These methods, however, can handle only the

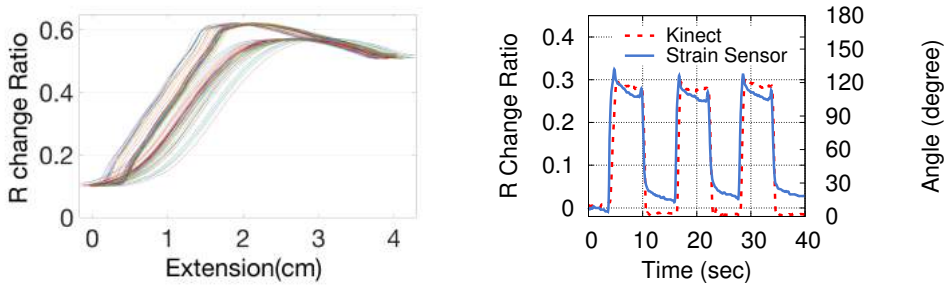

(a) Instability of resistance change (b) Stress relaxation

Fig. 6. The impact of stress relaxation (a) and the instability of resistance change in 160 rounds of stretching (b).

initial offset caused by wearing, not the error during the motion. We aim to seek solutions that are robust against slight position offsets of the sensing fabrics during joint motions.

4 SYSTEM DESIGN

We address above challenges via four key design elements:

- **Augmentation with Pressure Fabric**: to tackle the lack of one-to-one mapping between stretch length and resistance change, we augment strain fabrics with collocated pressure fabrics. Sensing the pressure from the joint motion, pressure fabrics are less sensitive to subtle joint motion and exhibit a narrower sensing range. However, they offer robust differentiation of coarse motion states (loading/extending, unloading/retracting, motionless). Once the motion state is identified, the system can select the proper modeling on strain fabric's resistance change for inferring the actual skin deformation.
- **Gaussian Distribution Curve**: Instead of relying on a single function to characterize the resistance change ratio under varying stretch length, we study the *distribution* of resistance change ratios to address the instability problem. Applying a statistical graphical method (Quantile-Quantile plot), we validate that the distribution is Gaussian. We then design a probability-based method to infer the extension length.
- **Modeling Stress Relaxation**: we model fabric's stress relaxation by leveraging the literature from material science. We first apply the classical spring-dashpot model [36, 66] to characterize fabric's resistance change. We then model the stress relaxation via a relaxation modulus and use the model to compensate for the resistance decline during stress relaxation.
- **Dual Strain Fabrics for Inferring Joint Angle**: we derive the geometric relationship between skin deformation and joint rotational angle based on the anatomy of joints in biomechanics. We propose the use of two parallel strain fabrics separated with a fixed interval and examine the difference between the two fabrics to cancel out the impact of fabrics' motion artifact and robustly infer joint angle.

Figure 7 illustrates the overall system flow. We next describe each element in detail.

4.1 Augmentation with Pressure Fabric

Our first design element augments strain fabric sensing with pressure fabric to disambiguate motion states. Pressure is created by the squeezing of body joint and sensing fabrics. Pressure alone does not lead to precise sensing of joint motion. However, it can serve as an instructive reference to differentiate coarse motion states. We consider collocating strain fabrics and a small piece of pressure fabric (the actual placement is described in §5), so that they respond to the same joint motion and complement each other's sensing ability.

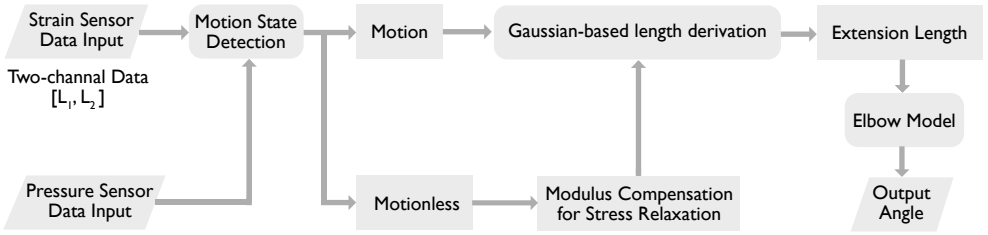

Fig. 7. System design overview.

Characterization of Pressure Fabric. Pressure fabric commonly contains velostat, linqstat or other piezo-resistive materials whose resistance changes under pressure. Prior works have explored various layouts of such fabric, including grid [63], circle [88], and stripes [72]. Pressure fabric is known to exhibit poor resilience and random signal drift because of its unsatisfactory mechanical property of the dieletric polymer layer [45, 80]. Thus, it is not suitable for accurately sensing subtle motion. However, its superior binary distinguishable upper and lower bounds with its linear slope enables it to be qualified motion monitor. We place it on the top of the bulge formed by bending a joint, so that it differentiate coarse motion states such as flexion and extension.

We have tested various materials (velostat [71] vs. NW170-SLPA-2k by EeonTex [70]), number of layers, and material of electrodes (woven conductive fabric vs. NW170-PI-20 by EeonTex [69]) as the pressure fabric. The results of various configurations are shown in Figure 8. We observe that overall, resistance decreases when the fabric is pressed, leading to negative resistance change ratios. Resistance changes more significantly with more layers. Changing the conductive cover from NW170-PI-20 to woven conductive fabric results into noisier resistance values. The reason could be the porosity of woven fabric causes poor contact with the pressure sensitive material. NW170-SLPA-2k pressure sensitive fabric by EeonTex exhibits the smallest resistance change given the same pressure. Thus, we settle on the two-layer structure with velostat in the middle as the pressure-sensing material.

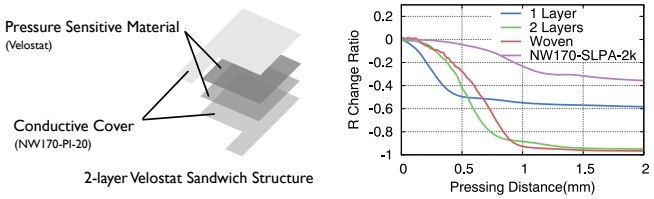

Fig. 8. Examining the property of resistance change with various pressure fabrics.

Disambiguating Motion States. Based on pressure fabric's resistance change, we aim to differentiate two motion states (*loading*, *unloading*) and a *motionless* state. Disambiguating these states is essential as each state corresponds to a different modeling of strain fabric's resistance change. Once a motion/motionless state is identified, the system can later apply the correct model on strain fabric's resistance change to derive the actual skin deformation (i.e., stretch length).

The differentiation of these motion states is based on the observation that joint flexion during loading raises the pressure sensed by the fabric (thus lowering the resistance), whereas joint extension during unloading lowers the pressure at the fabric (thus raising fabric resistance). Motionless states lead to relatively stable pressure at the fabric. Therefore, these motion/motionless states can be detected by examining the first-order derivatives of the pressure fabric's resistance change over time. A negative derivative indicates joint flexion/loading, while a positive derivative indicates joint extension/unloading. A derivative close to zero indicates motionless states.

Directly computing derivatives over pressure fabric's raw data, however, is prone to errors, given that sensor data are noisy and fluctuate over time. The noise can be introduced by the slight movement of the fabric over skin, or by the lack of sufficient force to the body [30, 55, 67]. To deal with sensor noises and ensure a robust detection, we smooth the raw data within a sliding window, interpolate data points between adjacent data points, and then compute the derivatives with the interpolated data points to obtain a more accurate trending of the raw data. Specifically, we have examined three algorithms for data smoothing: a) Savitzky Golay fitting, which is inspired by Savitzky Golay filter [84] algorithm. We simplified its curve fitting for our real-time computation; b) Local regression fitting, which is built upon a weight function that assigns the highest weight to the data points nearest the point of estimation [83], and c) Gaussian kernel fitting, an algorithm whose core is widely used Gaussian kernel [82]. Results show that Gaussian kernel fitting achieves the best tradeoff between accuracy and computational complexity. §6 presents detailed comparison of these algorithms.

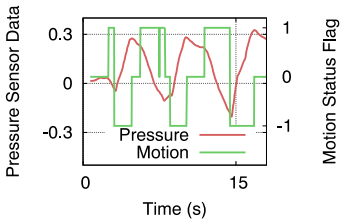

Fig. 9. Detection of motion states.

Algorithm 1 lists the detail in differentiating motion states, where $\hat{x}$ denotes interpolated data points. Data from pressure fabric are first fed into a circular buffer where the pointer to the data moves circularly, so that we can decrease the lag caused by real-time computation. Then we smooth the data in the buffer within a sliding window avoiding mutation in sequential data stream. Next, for the newly updated buffer, we interpolate data points based on the discrete data points in the buffer and then compute the first derivative with the interpolated data points. We compare the derivative k_t to a threshold k_{Motion} to determine if it is a motionless state. We then examine the sign of k_t to differentiate loading and unloading states. Figure 9 shows an example run of the algorithm, where 1 means loading, -1 denotes unloading, and 0 means motionless states. For motionless status, pressure fabric data are further compared with two pre-set thresholds to decide whether the state is motionless with strain or without strain. With the identified motion state, next we describe the modeling of strain fabric's resistance change to derive the stretch length (i.e., skin deformation).

ALGORITHM 1: Detecting Motion States.

Input: Data from pressure fabric x_t.
Output: Motion state: loading, unloading or motionless.
buf: circular buffer;
b: input scale of Gaussian kernel;
repeat
  Motion = Motionless;
  insert new data into the circular buffer;
  for *each buf updated by new data* x_t **do**
    $\hat{x} \leftarrow$ data interpolation;
    Gaussian kernel ($\phi(\hat{x}, x_t) = exp\left(-\frac{(\hat{x}-x_t)^2}{2b^2}\right)$) regression on the buffer buf with param b;
    calculate the slope k_t of current curve at data point x_t;
    if $|k_t| < k_{Motion}$ **then**
      continue;
    else
      $k_t < 0 \rightarrow Motion = Loading$;
      $k_t > 0 \rightarrow Motion = UnLoading$;
    end
  end
until *no more data point comes in*;

4.2 Derivation of Stretch Length

The second design element aims to infer stretch length based on fabric's resistance change. Given the instability of resistance change across repeated stretch cycles, we examine the distribution of resistance change ratios under a given stretch length across different rounds of stretch. Based on the characteristics of the distribution, we design a probability-based method to infer the stretch length. We next describe our analysis of the distribution and the probability-based method in detail.

Distribution Analysis. Earlier results indicate that the same level of strain (i.e., stretch length) can lead to different resistance change ratios across repeated stretches (Figure 6(a)). We set out to analyze the distribution of resistance change ratios under a given stretch length. We conducted 160 rounds of stretch experiments on the tensile test machine while sampling fabric's resistance change ratio at 100 Hz. In total, we obtained 160 data points (i.e., resistance change ratios) for each stretch length. We stretch the fabric by up to 4 cm, with 0.1-mm interval, resulting into 400 stretch lengths. For each stretch length, we analyze the distribution of resistance change ratios. Using a statistical graphical method (Quantile-Quantile plot), our results reveal that the distribution is Gaussian. Quantile-Quantile (Q-Q) plot is a probability plot, which compares two probability distributions by plotting their quantiles against each other [86]. Here we fix one probability distribution as the standard Gaussian distribution and compare each distribution with it. Figure 10 shows an example. We observe that the points distribution is almost linear, suggesting that the distribution of resistance change ratios under a stretch length is Gaussian [31].

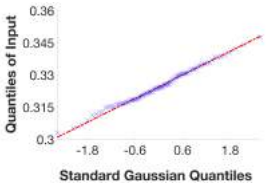

Fig. 10. Q-Q plot of sample data vs Standard Gaussian distribution.

Probability-Based Length Derivation. We exploit the Gaussian distribution of resistance change ratios for each stretch length to infer stretch length. Specifically, for each stretch length, we derive the mean and variance of the Gaussian distribution of resistance change ratios and store them in a look-up table. We then divide the look-up table to four classes, which are resistance increase during loading, resistance decrease during loading, resistance increase during unloading, and resistance decrease during unloading. Upon a sensed resistance change ratio, we first determine the class it belongs to based on the slope-based method and the output of pressure sensor. We then calculate its corresponding stretch length as well as probability based on each Gaussian distribution. The length with the maximal probability is selected as the inferred stretch length. Algorithm 2 lists the detailed steps.

ALGORITHM 2: Extension length derivation.

Input: Data from strain fabric x_t and motion state ($Motion_1$): loading/unloading
Output: Extension length.
buf: circular buffer;
repeat
  insert new data into the circular buffer;
  for *each* buf *updated by new data* x_t **do**
    slope-based method → $Motion_2$ = increasing/decreasing
    Combine the $Motion_1$ and $Motion_2$ → MotionClass;
    for *each distribution in this class* **do**
      calculate the probability P_i
    end
    find the maximum probability P_{max};
    return the extension length corresponding to P_{max}.
  end
until *no more data point comes in*;

State	MSE	RMSE/cm
Loading_increase	0.0063	0.0792
Loading_decrease	0.0168	0.1292
Unloading_increase	0.0231	0.1518
unloading_decrease	0.0204	0.1428

Table 1. Average MSE and RMSE of inferred extension based on leave-one-out cross-validation for strain fabric 1.

State	MSE	RMSE/cm
Loading_increase	0.0045	0.0674
Loading_decrease	0.0084	0.0918
Unloading_increase	0.0211	0.1452
Unloading_decrease	0.0046	0.0676

Table 2. Average MSE and RMSE of inferred extension based on leave-one-out cross-validation for strain fabric 2.

Validation. To validate our length derivation algorithm, we use leave-one-out cross validation to evaluate its accuracy. In each fixed extension length, we have collected 160 resistance change ratios. We use 159 values to calculate the mean and variance of one particular Gaussian. For 400 stretch lengths (i.e., Gaussian distributions), we set the MotionClass of these 400 points and run Algorithm 2 to derive the stretch length. We calculate the mean squared error (MSE) and root mean squared error (RMSE) for each extension length. We summarize the results of two strain sensors in table 1 and table 2, respectively. We observe that the algorithm's RMSE for each motion class is around 0.1 cm, which demonstrates that our algorithm performs well in mapping the resistance change ratios to extension lengths.

4.3 Modulus Compensation for Stress Relaxation

The third design element aims to compensate the stress relaxation. With the second design element, we can derive the extension length in motion states. For motionless states where stress relaxation occurs, we apply relaxation model from the literature of material science to compensate for the impact of stress relaxation. Its core lies in the characterization of strain fabric's resistance change.

For most typical polymers whose conformational change is eventually limited by the network of entanglements or other types of junction points, a classical "spring-dashpot" model is effective to analyze its properties [36, 56, 66, 90]. Here, since we add an additional layer of elastic material parallel to the sensing material, we choose Maxwell form (instead of Kelvin-Voigt form) standard linear solid model to describe our strain fabric [85]. As shown in Figure 11, the model is composed with a spring-dashpot branch and another spring placed parallel with the branch. We mark the stiffness of two springs as k_1 and k_2, while that of dashpot is η. If we further denote the stress on the system as σ and deformation as ϵ, based on the basic rule of spring and dashpot ($\sigma = k\epsilon$ and $\sigma = \eta\epsilon'$), we can derive the constitutive equation of this system as:

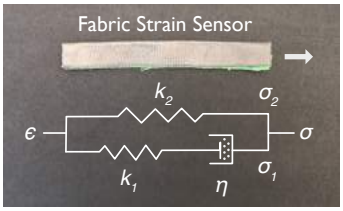

Fig. 11. Approximating a strain fabric using a spring-dashpot model.

$$\sigma = \sigma_1 + \sigma_2$$

$$\epsilon = \epsilon_1 = \epsilon_2$$

$$\rightarrow k\epsilon' = (k_1 + k_2)\epsilon' = \sigma_1' + \frac{1}{\tau}\sigma_2 \tag{2}$$

where $\tau = \frac{\eta}{k_2}$ is called relaxation time constant. Such constitutive equation links deformation to the stress on the material, and the solution of this differential equation is in exponential form ($a + e^{bx}$). We will make use of it in the following part.

Since in stress relaxation, $\epsilon' = 0$, equaion 2 becomes:

$$\frac{d\sigma}{dt} = -\frac{1}{\tau}\sigma \tag{3}$$

Separating variables and integrating we can get:

$$\sigma(t) = \sigma_0 e^{-\frac{t}{\tau}} \tag{4}$$

Then the relaxation modulus $E_{rel}(t)$ can be derived as:

$$E_{rel}(t) = \frac{\sigma(t)}{\epsilon_0} = k_2 + k_1 e^{-\frac{t}{\tau}}, \tag{5}$$

where τ, as *relaxation time*, is the key parameter that we use to compensate for relaxation. We fitted the relaxation model with experimental data, and specific parameter values are listed in footnote [1].

4.4 Inference of Joint Angle

With the derived stretch length, the last design element is to infer the joint angle. We analyze the anatomy of human joints to identify the relationship between the deformation and the rotation of joint bones. We then discuss the use of dual strain fabric sensors to enhance sensing robustness.

Human joints can be categorized into six types: synovial joint, pivot joint, hinge joint, saddle joint, condyloid joint and ball and socket joint. Elbow joint is categorized as hinge joint, where the bones can only move along one axis to flex or extend. [68] Its moving range is around -10° to 150° [43], and some works from anatomy have confirmed the relationship between the skin surface deformation and elbow flexion angle [24, 41, 54]. Here, what we have got in the previous steps is the extend length on the fabric caused by skin deformation, and now we need find a method to link the skin deformation to the rotation angle.

If we take a close look at the elbow joint, three bones are involved in the rotation at the elbow joint: humerus on the upper arm, radius and ulna on the lower arm.

Fig. 12. Anatomy of the elbow joint.

As shown in Figure 12, the distal end of the humerus and the proximal heads of the radius and ulna form a small flat triangle-like surface, that is also supported by the collateral ligaments around the elbow. When we wave our arm, the ulna, definitely with its upper end (called olecranon) will rotate around a virtual rotation axis, and as a result, the triangle-like surface will also rotate in a certain range.

The rotation of this surface causes the deformation of skin around the joint. Prior studies have proposed models to describe the relationship between skin deformation and joint rotation [59, 65, 75, 76, 78]. The common problem of all these models is that they assume the virtual rotation axis of the ulna's rotation is known or easy to measure, which is hard in practice to locate because the axis is above the skin and the height is unclear. Another problem of these models is that they assume the bulge (i.e., olecranon) of the joint is a perfect horizontal surface, while in fact it tilts with a slope that depends on the shape of the joint bones [20, 28, 92]. To solve all these problems, we

[1]The three parameters of our relaxation model are:0.0233, -0.04591, 0.0289. SSE:0.0795, RMSE:0.01154.

apply a general model in terms of anatomy that can cover different joint sizes. We tackle the problem of rotation axis localization with two parallel pieces of strain fabric.

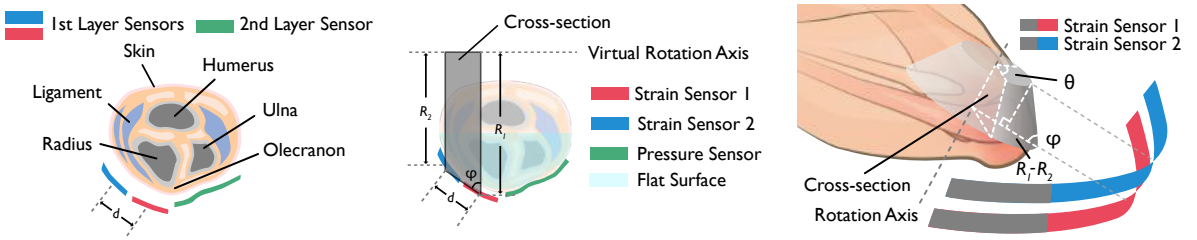

(a) Two layers of sensing fabrics on the elbow: pressure sensor and strain sensors

(b) A trapezoid cross-section (grey) formed around the virtual rotation axis

(c) A circular truncated cone formed by the rotation of cross-section

Fig. 13. Inferring the joint angle based on the stretch lengths sensed by two strain fabrics. (a) Pressure sensor on the first layer while two strain sensors on the second layers. (b) We denote the orthogonal distances between strain sensors and virtual rotation axis as R_1 and R_2. The two radius, the virtual axis and skin surface slope will form a trapezoid cross-section. The flat surface is also plotted for reference. (c) The rotation of the cross-section will form a circular truncated cone whose top surface radius is the deformation of strain sensor two and base radius is that of strain sensor one. Its height can be computed with distance d and angle ϕ.

Sensor Layout. Figure 13 (a) and (b) show our design on sensor layout. We adopt a two-layer structure to put the two kinds of sensors: the first layer, which is more closed to the skin, is the pressure sensor who is responsible for the status judgement, and the second layer, which is exposed to the outer, is the two strain sensors. Figure 13 (b) shows the cross-section (grey trapezoid) that rotates with elbow movement. First we mark the virtual rotation axis with dotted line. As we mentioned previously, its location is unknown and we just randomly pick a position. Then based on the location of axis, we draw two orthogonal radiuses whose distal ends are two strain sensors. Finally we could see that there is a trapezoid shaped cross-section above the two strain sensors. We denote the two radius as R_1 and R_2, and the distance between them is d. We also consider the inclination angle of flat triangle surface (we mentioned previously) as ϕ. R_1 and R_2 are two unknown parameters, while d and ϕ are body parameters that we can measure during calibration. We will talk more about the measurement procedure in the evaluation section.

Dual Input Sensing. Figure 13 (c) illustrates how we infer the movement angle with all the parameters we set in the previous step. The extension on the two parallel strain sensors can be seen as two arcs of one virtual circle (whose center is the virtual axis). We denote the length change of each arc as L_1 and L_2 (i.e., stretch lengths of the two strain fabrics) and the joint angle as θ. Note that if we view from the projection direction (as shown in Figure 13 (c)), the rotation of the cross-section will become a circular truncated cone. With all these parameters, the joint rotation angle θ can be computed as:

$$\theta = \frac{L_1 - L_2}{R_1 - R_2} = \frac{L_1 - L_2}{d \cdot \cos(\phi)}, \tag{6}$$

where d and ϕ are calibrated parameters, L_1 and L_2 are the stretch lengths sensed by the two strain fabrics. Thus, we avoid the potential error imported from inaccurate estimation of rotation axis and the radiuses (R_1, R_2). Furthermore, the use of two pieces of strain fabric also allows the system to be robust against small position offsets of these strain fabrics during joint motion. Since the derivation of joint angle in Eq. (6) uses the difference of two stretch lengths, small position offset of the strain fabrics is canceled out, given that the two strain fabrics are collocated on roughly the same slope of the skin.

We calibrate parameters d and ϕ based on a user's bone shape and tissue distribution. First, depending on user's joint size and thickness, the distance d between the two strain fabrics can be slightly extended as a user

puts on the prototype around a joint. The actual value of d can be measured during a user's first wear of the prototype. Second, ϕ, the slope of the flat surface around a joint, can differ across users. Since it is not easy to directly measure it on the skin surface, we calibrate it by asking the user to perform a full flexion of a joint, i.e., transitioning from full extension to full flexion. Given the maximal rotational angle $\theta^\star$of a joint (e.g., the maximal rotation of an elbow joint is around 150° [24, 61, 76]), the angle ϕ can be computed as $\phi = \arccos \frac{(L_1' - L_2')}{d\theta^\star}$ based on Eq. (6), where L_1', L_2' are the stretch lengths of the two strain fabrics during the full flexion. For both parameters (d and ϕ), their values stay relatively constant for a given user. Thus, the system requires only an one-time calibration for a user, instead of a calibration for every wearing instance even with the same user, entailing a lower calibration overhead than prior works [47, 48, 60, 65].

5 PROTOTYPE IMPLEMENTATION

We build two prototypes in different sizes using stretchable conductive fabric as strain sensor, inelastic fabric as reference resistor, pressure-sensitive conductive sheet as pressure sensor, stainless steel conductive thread as wires, micro-flex compression knit fabric as layers, sewable snaps and iron-on adhesive hem to connect, sports kinesiology tape to insulate, and a micro-controller (Adafruit Flora). Instead of inventing new high-cost materials, all the components in the system are easy to obtain and at low prices (<$20 except the micro-controller). While aiming to optimize the performance, we also guarantee that the device is comfortable to wear and washable.

5.1 Sensing Fabrics

Layers. We hand-cut two pieces of non-conductive micro-flex knit fabrics [39] to act as two layers. Layer 1, the pressure fabric is placed in the inner layer close to the skin so that its resilience can be supported by the outer layer, while layer 2, the strain fabrics are placed in the outer layer for the maximal degree of extension. This two layer design structure has two advantages: 1) It provides physical isolation between pressure sensor and strain sensor, so that the deformation on the fabric strain sensor will not be limited by the inelastic pressure sensor. 2) Borrowing idea from PCB manufacture, such double-layer structure can spare more room for conductive thread to connect different parts because the thread has access to two surfaces now with the help of some connecting holes. For the first advantage, our early-stage prototypes confirmed that, if we put the sensors in the same layer, the closest strain sensor to the pressure sensor can hardly respond to strain because of the shared gap with pressure sensor, though the gap itself is flexible. For advantage two, such design makes the implementation of prototype much easier and also it reveals stronger anti-interference ability than one-layer version, since there is no cross or squeeze of conductive thread on the surface even if we do vigorous movement. The sensing fabrics on two layers are totally independent and well-insulated from each other. The only connection between the two layers are three conductive sewable snaps so that the circuit on Layer 1 also gets power supply and transmits voltage value to the micro-controller.

Strain Fabrics. We use LessEMF #A321 [37] as the stretchable conductive fabric, which is silver plated with 76% Nylon and 24% elastic fiber fabric. Our experiments show that a single-layer strain fabric does not offer mechanical stability after repeated stretches, leading to large fluctuating peaks of resistance change ratios over time (Figure 14(a)). To address this issue, we design a two-layer structure, where we paste a layer of insulative elastic tape (KTape [15]) atop the LessEMF fabric, fold it with KTape in the middle and LessEMF on the top and bottom, and then sew these layers with elastic zigzag stitches. The strain sensing fabric is cascaded with an inelastic conductive fabric (EeonTex NM170-PI-20 [69]) serving as the reference resistance. The reference fabric has a similar two-layer structure and layers are sewed using simple inelastic stitches. Figure 14(b) illustrates the fabrication process. Such a two-layer structure improves the stability of output voltage (Figure 14(c)). With KTape in between, it also provides insulation that mitigates resistance shift. Specifically, strain fabrics (LessEMF)

are cut into pieces of 15 cm × 3 cm in size, resulting into 1.5cm width sensing fabric after the folding. It is then connected to a 7 cm × 1.5 cm static conductive fabric (EeonTex NM170-PI-20) as the reference resistance. We sew two strain sensors onto Layer 1 using zigzag stitches, which do not influence the elasticity of sensors. They are the main sensing fabrics in our prototype and are placed roughly in accordance to the flat surface of elbow. One important part of making the strain fabric is to find suitable resistance of the fabric. Due to the large surface of the conductive fabric, the resistance value fluctuates. We noticed that the fluctuating range is around 1% of its original resistance, which means smaller resistance value will cause less fluctuation.

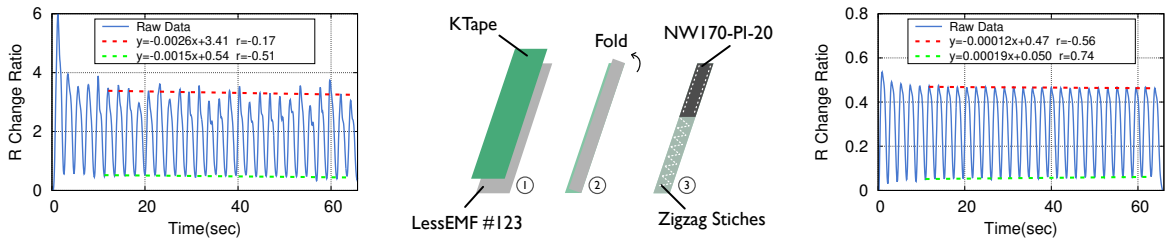

(a) One-layer structure (b) Fabricating two-layer strain fabric (c) Two-layer structure

Fig. 14. One-layer strain fabric leads to mechanical instability over repeated runs (a), while a two-layer structure (b) provides much more stable output (c).

Pressure Fabrics. Triple-decker structure is applied to the pressure fabric. We place a 3 cm × 4 cm piece of static conductive fabric at the bottom, another 3 cm × 7 cm one on the top and two 3cm×4cm pieces of 1mm-thick pressure-sensitive conductive sheet [71] in between. Both the top and bottom layers perform as reference resistors and have an extra part as pins to connect with conductive threads. We use iron-on adhesive hem to stick them together and cover the sensor with kinesiology tape to fasten and insulate. As pressure that elbow exerts on the sensor without any supporter contributes more to spatial deformation rather than forming a sagging area , we sew a piece of stretched highly-elastic fabric [38] outside the sensor unit to provide a reversed pressure while bending arms. Pressure sensor is laid on Layer 2 beside two strain sensors on Layer 1 and exactly covers the olecranon part of elbow 4.4.

It is worth mentioning that when we use conductive thread as the wire to connect the pressure sensor with snaps, the intersection part between the threads and sensor need to add a piece of conductive elastic fabric. This is because the pressure fabric is inelastic, which will leave much more gaps between threads and fabric, causing the resistance sharply increase. As we use the change ratio to determine the loading or unloading state, the absolute value of the resistance cannot be too large, or the sensitivity will be too small to differentiate. Another tip for sewing is that since the condctive thread is too thick to go through the hole of the sewing machine, we put it in the bottom bobin.

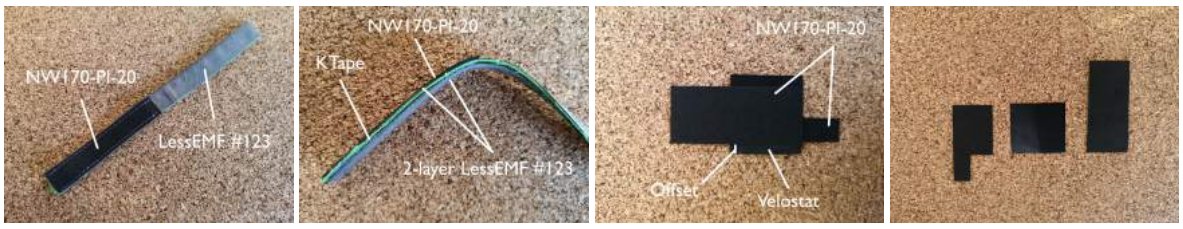

(a) Two-layer strain fabric (b) Two-layer strain fabric (side) (c) Two-layer pressure fabric (d) Pressure fabric components

Fig. 15. Strain and pressure fabrics.

(a) Layer 1 (inner layer) (b) Layer 2 (external layer) (c) Final look

Fig. 16. Integrating strain and pressure sensing fabrics into regular elastic fabrics.

	Sex		**Height/cm**			**Weight/kg**		
	Male	Female	<170	170 - 180	>180	<60	60 - 80	>80
# of Users	7	3	2	4	4	3	4	3

Table 3. Participants information in evaluation study, where participants differ in height and weight.

User ID	1	2	3	4	5	6	7	8	9	10
Upper Arm Size/cm	31	29.5	30	32	27.5	23	24.5	22.5	23	23
Lower Arm Size/cm	27	22.5	23.5	24	24.5	21.5	25	23	20.5	22

Table 4. The upper and lower arm size of 10 participants.

5.2 Computing Unit

We use an Adafruit FLORA v2 board whose core board is ATmega 32u4 to digitize analog voltage signals of each sensor. FLORA is a small (1.75" diameter, weighing 4.4 grams) and fabric friendly board with sewing tap pads, which interferes little with motions and can be sewed on the sleeves. ATmega 32u4 is a 8-bit micro-controller with 32K bytes of ISP Flash. During signal digitization, we use 250kHz ADC rate, which is sufficient in capturing low-frequency motions. Timer frequency is 100Hz and real-time interference results are stored in the MCU.

We sew eight conductive snaps on the layers, among which three electrically connect two layers and five attach the sewing tap pads on Flora to Layer 1 so that the micro-controller is detachable. Also, we sew conductive threads into the layers as leads to connect three sensors with the micro-controller. To avoid unwanted signal inference, all the conductive threads which expose to the air are covered with sports kinesiology tapes. According to the contact resistance theory [35], contact resistance is proportional to the material hardness and inversely proportional to the number of contact points and the contact pressure. Therefore, given that EeonTex static conductive fabric is a kind of hard material, we add intermediary pieces of stretch conductive fabric in all the connections between conductive threads and static conductive fabric.

6 EVALUATION

We recruit 10 participants (7 males and 3 females) to evaluate our system. We summarize the user information in Table 3. Four of them wear the big-size prototype while the others wear the smaller one. In this section, we will first focus on the overall accuracy across all users. Then we will examine its performance given specific pattern of movement. Next we will have a look at its reliability given sensor moving. Finally, we will talk about its comfort level rated by all the users.

Setup. Although our device has the ability of self-adaptive to different sizes (it is flexible, and its model is based on bones instead of soft tissue), it has to be tightly worn so that the pressure sensor can detect considerable signal change during the movement. Given that our testers cover a wide range of sizes, we have to fabricate another size prototype to fit in stronger testers whose upper arm size is larger than 24cm. In Table 4 we list all measure results of testers' upper and lower arm size. The range of upper arm size is 8.5cm while that of lower arm is 6.5cm. Before the test, we will ask them to roll up their sleeves and measure their arm size to find proper prototype to wear. To instruct testers' movement, we recorded a video and let testers imitate the movement flow in the video to guarantee that different testers have nearly identical patterns of movement. During the test, we broadcasted the next move so that the testers can make a rapid response to the instructions.

Ground Truth. We use Vicon (Vicon Motion System Ltd. UK) [13] as our ground truth because of its higher accuracy in comparison to other motion-capture systems such as Kinect. Its sensing ability relies on the reflective skin markers and infrared cameras and the system error is less than 2 mm [52]. We attach optical markers to participant's elbow to measure the skin deformation and elbow angle. In our early-stage tests, we found that if we attached three markers to the arm (on upper arm, elbow joint and lower arm respectively), sometimes Vicon would lose track of the markers (because markers could be sheltered by body at times during large movement). Instead, we created two rigid plane with hard paper board and placed them onto the upper and lower arm skin surface, so that Vicon can easily track the two rigid objects and outputs the angle between them even if one or two points on the plane is missing. Meanwhile, in order to synchronize and compare data from Vicon and our device in real-time, we developed a cross-platform tool with C language to gather data from MCU and Vicon system together and we integrated calibration procedure into the tool. The whole time of one-person test takes about 40 minutes with calibration and adjustment taking only three minutes.

Evaluation Flow. The whole procedure of our evaluation can be divided into four steps.

(1) Given magnitude (90°), do the movement at three levels of speed, and given speed, do three magnitudes (45°, 90° and 150°) of movement. Repeat every movement three times. Rest 30 seconds after this step.
(2) The pattern of movement is the same as the first step, but stop at the end of each movement for five seconds. Rest 30 seconds after this step.
(3) Stop and restart to move at four magnitudes (0°, 45°, 90° and 150°) at two speed levels and with two length of stop time (one second and five second), so in total there are four loops in this step. Rest ten seconds between this four loops.
(4) Practical movement, including waving tennis racket, tree pose from yoga and belly button challenge for testers.

The first step is mainly to see the calculation accuracy of our model. We are curious about that because our strain sensor has non-linear model and we use fabric pressure sensor as fusion to help us decide the solution region. We set three magnitudes and three speed levels for the movement so that we can know whether the model we derive in design section 4.3 is reliable and steady enough under different movement. Another reason for setting these six cases is we are trying to find some relationship between accuracy and different speed levels or magnitudes. For the second step, with five seconds stop at the end of movement, our purpose is to look at the stress relaxation and drift compensation performance of our fabric sensor system.

In addition, we are curious about its behavior when we resume moving from a certain strain level. For example, tester stops at 45° for five seconds, and then continues moving to 90°. Since the deformation on the strain sensor is calculated from a non-linear model and it suffers drift and relaxation problem within the five-second stop, it may accumulate some error when it moves to next spot. Thus we set a three-step (45°, 90° and 150°) stop-and-restart experiment as our step three, with two speed levels and two waiting time options, hoping that we can have some insight about its error caused by accumulation.

Moreover, we prepared three kinds of practical movement: 1) waving a tennis racket several times, to check the performance of our system at high speed and in large range of motion; 2) tree pose from yoga, to see the ability of reconstructing motionless and steady gesture. 3) belly button challenge, a popular movement among the young people around the world that can test flexibility, which requires using one hand to touch your belly button from the other side across your back. We expect to see similar performance when the elbow movement is done with some full-body motion.

The test lasts 30 minutes. For user study, we also composed a questionnaire containing ten questions to know the experience of the experiment (like comfort level and wearing habit) and others aspects of our interests. The answers to these questions are all on a scale of one to ten. Besides questionnaire after test, we purcahsed several best-selling compression sleeves for our testers as comparision. In the following part we will summarize testers' answers to these questions and put forward a plan of our future work.

6.1 Sensing Accuracy

We view accuracy performance in three aspects: 1) overall accuracy, where we use the data from the above four steps from each user, in order to summarize the accuracy performance across the whole experiment; 2) accuracy of specific movement setting, where we will select certain criterion (magnitude, speed and etc.) as the only parameter to analyze our data; 3) accuracy in terms of user diversity, where we will category tester into several groups and try to find out accuracy pattern given body parameters.

6.1.1 Overall Accuracy. The overall accuracy is to examine our system in a comprehensive movement setting. The movement designed in the evaluation flow section will be all contained in our overall test movement set. We plot results of ten participants in 17 and the overall average accuracy is 9.69°. We also categorized users into three arm size groups: small (upper arm size < 24cm), medium (24cm ≤ upper arm size ≤ 28cm) and large (upper arm size > 28cm). The reason why we chose upper arm size as the standard is that the elbow is closed to the upper arm end of our prototype while lower arm end nearly has no influence to the tightness of wearing. From the result, we found that the medium arm size performed best among the three, which can be partially explained by the tightness best fitting medium users. We also have a look at whether the male shows different behavior from the female. As shown in Figure 17 (c), there is no big difference between the two genders.

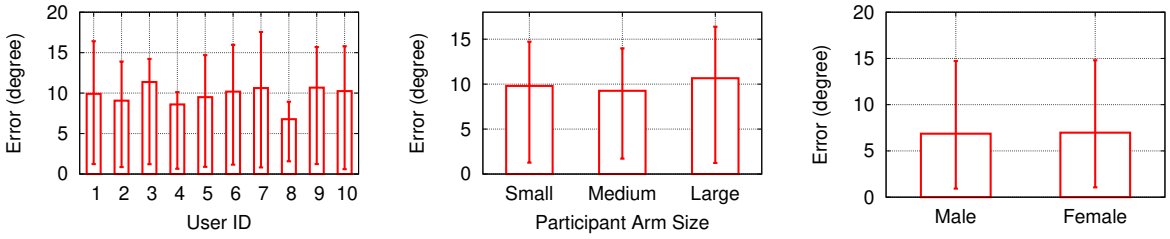

Fig. 17. Overall reconstructing performance: (a) all participants; (b) different arm sizes; (c) male vs. female.

6.1.2 Specific Movement Pattern Accuracy. In this section, we will focus on specific movement pattern that we defined in experiment flow part. We will compare the performance under different stop time, speed and magnitude and give our explanation.

Stop vs. Non-stop. Figure 18 (a) shows the CDF curve of error that belongs to "stop with five seconds" and "non-stop". We observe that the reconstructing error distribution in two settings is nearly identical, where the median error is around 10 °. It means that our system can deal with time-dependent behavior very well with

(a) (b) (c)

Fig. 18. Reconstructing performance given specific movement pattern: (a) stop and non-stop; (b) three levels of speed and (c) magnitude.

our stress relaxation and drift compensation algorithm. However, non-stop group can touch maximum error (38.7°) while that of stop group is 34.3°. The reason could be that the non-stop pattern, with arm immediately getting back after the movement, introduces some vibration on the fabric strain sensor. In that scenario, since our testers did movement in a continuous way, sometimes it is hard for them to keep controlled at the end of each movement. The shaking of their arm will result in the vibration on the fabric strain sensor. That's why we observed such peak-like error in the CDF curve, but in general, it is reasonable to reckon that our system managed to handle the holding status during the movement.

Speed. Speed is another factor that may affect our system performance. We evaluated our prototype with three speed: Lowest speed (20 degree/s), edium speed (50 degree/s), Highest speed (80 degree/s). As shown in Figure 18 (b), it is apparent that higher speed causes worse accuracy performance while lowest speed has over 80% confidence that its error is within 15°. Given that the modulus we use for stress relaxation and drift is time-dependent, it is likely that the relaxation is loosely related to speed. Another possible reason is that for higher speed, the fixed window (12) on motion detection algorithm may be not wide enough for the regression kernel to reconstruct the curve. The confused motion detector may output some unreliable motion status at high speed. In the future, we plan to develop a self-adaptive windows size selection module based on current speed before our motion detection part. It is challenging as well since the practical movement is not controlled and speed can vary every moment. One of the focuses of our future work could be how to identify the speed parameter in a reasonable way.

Magnitude. Figure 18 shows the accuracy results from three levels of magnitude. In our settings, the three levels are expected to be 45°, 90° and 150°, but there is definitely some variance in their practical movement. The result reveals that smallest magnitude has the best performance among the three, and the worst one, that moves to 150° has an median error of 9.24° and 20.21° at its 95-th percentile. We conclude this trend as the increasing complexity of computing reconstructing result. For smallest magnitude, there is no need to get the pressure sensor involved in because such little deformation can be completely covered by the increasing region of strain sensor characteristic curve. However, for larger movement, it reaches or goes over the peak, where we need pressure sensor to tell strain sensor which model we should apply to it. The tiny lag between these two sensing mechanism and malfunction of our motion detection module could be the source of error for this scenario.

6.1.3 Practical Movement Accuracy. As shown in Figure 19, we concluded our results for practical movements in three aspects: a) In general, slow movements can achieve higher accuracy with our prototype, that could be because of the slow restoration procedure of the fabric given sudden strain. b) Since wearing our prototype is location-selected (actually we have suggested wearing location), some practical movements related to lower arm or wrist

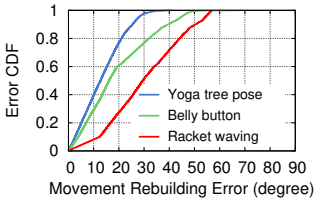

Fig. 19. Reconstruction error distribution with different practical movement

rotation may introduce error, especially in large angle area. For the curve of belly button, we can see that there is a slope indicating more high-value error than plain yoga tree pose, which means that when testers' start to rotate their arm to reach the belly button, our prototype meet difficulty to reconstruct the movement accurately. c) Big magnitude movement with high speed may bring about the most error in our system. During the test, we observed that sometimes the prototypes on testers became loose and moved to wrong location (though within 1cm) and there were wrinkles accumulated around their elbow, which is obviously not in best conditions. In a word, we recommend our users wear our prototype for small range movement (like yoga or indoor fitness) in a low speed.

6.2 Reliability

In the third part of our design section 4.4, we highlight the reliability of our system in two aspects: first, we make use of one-time calibration to obtain the body parameters that differs from person to person. We also consider about the influence from sensor moving and we solve it through anatomy knowledge. We calibrated every user before their test, and in the user study section we summarize their experience of the one-time calibration. The overall accuracy results can verify that our calibration method works perfectly.

Sensor Movement. For sensor moving problem, we set this dedicated evaluation step, where we tested accuracy of the same movement flow but at three different positions. Note that there is actually a suggested position for wearing, in order to make pressure sensor able to detect the compression around elbow. However, the sensing range of pressure sensor is still limited, so we the three positions we set for the test is almost the margin position the pressure sensor could work.

Figure 20 reveals the result. Given that the tester worn our prototype with his right arm, right movement does not cause much trouble for the pressure sensor. However, moving left will place the pressure sensor upon the soft tissue area that is crowded with ligament, tendons and fat. Another possible reason for the bad performance of moving left could be the strain sensor moves over the peak of olecranon, which means the two paralleled strain sensors are not attached to the same slope of the flat surface. That will definitely result in failure of calculating angle from differential input.

Fig. 20. Reconstruction error distribution with various sensor positions.

Washability. We implemented our prototype in terms of modular design rules, which means the computing part and sensing part are physically isolated and easy to be detached. As we mentioned in implementation part, we use conductive buttons as connector, which keeps MCU input pins and conductive thread in close contact.

Here we tested two levels of washing aiming to provide reasonable suggestions about how to properly wash our prototype in everyday use. We first washed it by hand slightly, and then we put it into washing machine to wash it in normal mode. We tested its reconstruction accuracy afterwards for each level and we also plot that of the original dry one as reference.

As shown in Figure 21, lightly wash has limited effect on the reconstruction accuracy, but for heavily washed one, its performance is quite unacceptable, since its median error is around 34.1◦ and its maximum error could reach 72.4◦. We carefully examined the reason why washing can such a big difference on our prototype, and we found that after the sensing fabric contacted water, even if we dried it thoroughly in open air, the fabric would shrink to some extent. Especially for the machine washed one, we observed that some conductive thread on it is broken and that can cause loose contact in our

Fig. 21. Impact of wash on fabric's sensing performance.

circuit on the fabric. Therefore, our suggestion for washing the prototype is to do hand washing and dry it in open air.

6.3 Comfort Level

To measure the comfort level of our prototype, we ask for feedback from 10 participates according to a questionnaire. We divide the level of comfort into four questions and participants give their answers with the scale of 1-9. First, we ask the participants to rate the tightness of our prototype (1-too tight, painful to wear; 9-very loose, do not feel wearing it at all). Second, participants rate the flexibility of our prototype (1-too rigid, cannot perform any motion; 9-very flexible, no hindrance to performing any activities). Third, we need to know the satisfaction of each participant on the one-time calibration at the beginning (1-too long, tedious; 9-quick, not an overhead at all). Finallly, each participant gives an overall comfort level of wearing our prototype (1-very uncomfortable; 9-very comfortable, do not mind wearing it at all times). The average values of the four questions are 6.1, 8.5, 8.3 and 8.8 respectively. It shows that our prototype turns out to have an acceptable comfort level: the sizes of our prototype well adapts to target users with different figures; The device does not hinder the motions for sports and everyday use; One-time calibration after purchasing it is relatively quick and acceptable.Besides, 9 participants think applying our device into the teaching process of certain sports like yoga or gymnastics is very helpful (8 points or more) to their progress and all the participants are willing to purchase such a device for $30-$40.

Besides getting the direct comments on our prototype, we collected their feedbacks on comparing the comfort level of our prototype with other regular fabrics. We invited participants to wear the off-the-shelf compression sleeves [1, 2] for 30 mins which is the same time of conducting the test. Overall, participants find no uncomfortable issue using our prototype. A participant comments that "There is no difference between wearing your prototype and the compression sleeves."(P5). They did anything they want during the wearing period. A participant comments that " When you are playing sports, this would not have any influence just as the protection arm sleeves, while it tightness might make you feel a little bit uncomfortable when you are typing before a computer."(P2)

7 RELATED WORK

We divide existing works into two categories based on their sensing capabilities.

Motion Classification Systems. Existing systems that use clothes itself, especially off-the-shelf fabric, as strain sensors are mostly for motion classification. Quite a few choices for fabric strain sensor can already be found on the market, and the most common category is resistive fabric sensor, whose electrical resistivity will change when mechanical strain is applied — this is called piezoresistive effect. There are two mainstreams of resistive fabric strain sensor.

The first one is textile structure with conductive yarn embedded strain sensor. The embedded conductive yarns form many conductive paths, where contact resistance would change following given mechanical stretch. Atalay et al. [16] chose to use silver yarn and nylon as the material and produced a weft-knitted strain sensor. Zhang et al. [89] created knitted strain sensors by using stainless steel and carbon yearns. The advantage of this kind of strain sensor is that the integration of the conductive medium into the textile structure is easily to be achieved by slightly modifying existing knitting machine procedure. Yet the mixture or the filling material of the sensing yarn is always something rigid, which may cause uncomfortable feeling while wearing. The other one is intrinsically conductive polymer (ICP) coated fabric strain sensor. Given that the wearable strain sensor has to suffer frequent deformation or even violent stretch, researchers use common elastic material (like lycra) as the substrates, coated with ICP, to obtain this new kind of strain sensor through chemical deposition method, etc. In 1997, Lorussi et al. [49] developed a PPy-coated Lycra fabric and presented a wearable system able to reveal the status of body kinematic chains. Oh et al. [57] coated PPy on Nylon-spandex(95:5) and obtained a strain sensor which can keep sensing until 60% extension. Irmandy et al. [81] used off-the-shelf PPy-coated fabric LTT-SLPA(28% Elastane, 72%

Nylon) made by EEONYX Inc. to develop a deformable musical keyboard. They suggested that the maximum strain the sensor could handle is around 100-150%, which indicates this fabric is ideal for wearable strain sensor as its working space is large enough for skin surface deformation happening on our body. However, none of these works focus on how to measure the accurate deformation of fabric or to obtain the numerical range of human motions. They can only realize some applications for pose recognition or human-computer interaction, which are based on binary or vague output. Without elaborate structures and efforts to eliminate the unfavorable properties of fabric, these fabric sensors cannot be ideal sensors for applications requiring high accuracy (like motion reconstruction), due to the random deformation-caused resistance change in practical use.

Project Jacquard [6], launched by Google at 2015, aims to turn clothes into wearables. Its highli ght product is a commuter trucker jacket (a product of Google and Levi's collaborate) that enables users to communicate through touch, tap and slide [7, 8]. All its functions rely on a "smart tag" at wrist, a sensor hub that gathers signals from the smart fabric, vibrates when receiving notifications, lights up in various colors indicating current status and so on [10]. One limitation of this jacket is that its touch sensitive fabric will malfunction after ten times wash. The reason could be that the Jacquard thread/textile is made of thin conductive metal alloys [9]. Another limitation is on its interaction method. Since its input comes from the gesture performed on the touch sensitive fabric, it is passively receiving actuation rather than actively detecting motion or interaction. There are a few pre-defined gestures that users can select to communicate with the smart tag, but other than those, Jacquard jacket fails to give feedback to input from real-time movements. Our work takes a step forward that we can not only do motion classification but also reconstruction with the help of real-time angle of joints.

Motion Reconstruction Systems. In early stage, works using strain sensors for reconstruction mostly relied on special-designed materials. Mattmann et al. [50] used a novel thermoplastic elastomer strain sensor and attached it to the back of a tight-fitting cloth to recognize upper body postures. Menguc et al. [51] pour liquid silicone on a 3D print mold and inject EGaIn to generate a soft strain sensor. Bae et al. [17] chose graphene, a special carbon structure as its base, made a transparent strain sensor detecting the motion of a finger. Ali et al. [40] designed functionalized fabric to measure triboelectric charges induced by fabric deformation, making it possible to differentiate joint movement types (extension, flexion) and movement speed with loose-fitting cloth. All these strain sensors require complicated chemical procedure and spectacular techniques, which is hardly at low cost and would limit its potential for mass manufacturing. Also, the reliability of such chemical substances in rigor environment can be a potential problem. Several prior work leveraged other materials instead of fabric to sense the joint movement. Peter et al. [29] incorporated conductive fibers into the fabric with elastic cord and sense the joint angle according to the resistance change of conductive fibers. Massimiliano et al. [26] made use of optical fiber, which measures the relative angle in a rotating joint based on the intensity modulation of a laser beam propagating in a single-mode optical fiber. Sunghoon et al. [46] developed a sensing system comprising a retractable reel, a string and a potentiometer. This system estimates the joint angle accurately under the fast movement settings with the help of the retractable reel. Other similar works like E-Skin by Xenon [14], on-body sensing system by FIGUR8 [5] and super soft stretch sensor by stretch sense [11]. Besides sensing fabric, E-Skin system places 3-axis accelerometer and 3-axis gyro sensor on the plastic part on the chest [3]. Stretch sensor attaches an extra circuit unit at the end of its smart garments [12]. Adrian [25] used the wearable inertial measurement units (IMUs) to estimate the movement skill. FIGUR8 claims to use 9-axis inertial measuring unit [4] in its products. Our work differs from above products because we reconstruct motion solely from on-body evidence (pressure and deformation) without any assistance from other sensing mechanism (accelerometer or gyroscope) and our work can blend with regular fabric easily, which provides an unobtrusive and comfortable approach to monitoring the joint movement.

8 CONCLUSION AND FUTURE WORK

We studied the use of off-the-shelf conductive fabrics to sense the strain and pressure during joint motion and infer joint rotational angle. We focused on addressing challenges arising from the inherent properties of fabric materials to achieve accurate and robust sensing. We leveraged models from material science and biomechanics to characterize fabric properties and the relationship between skin deformation and joint angle. We fabricated prototypes with off-the-shelf materials and micro-controller. We demonstrated system's sensing accuracy, robustness, and wearing comfort by conducting system experiments and user studies with 10 participants.

We recognize the limitations of our current study and summarize our ongoing and future work as follows:

- We currently fabricated prototypes only for the elbow joint. Moving forward, we plan to fabricate prototypes for other types of body joints and examine the efficacy of our design. The general design principle still applies and we will need to consider the anatomy of other joint types for possible adjustments on inferring joint angle. For joints such as wrists with larger degrees of freedom during rotation and capable of performing more types of rotational movement, we will consider optimizing the current design and arrangement of sensing fabrics to maximize the number of rotation types the system is capable of tracking.
- Since our sensing fabrics are conductive, sweat can affect their conductivity and interfere with fabric sensing. We have not noticed any participant sweating during the experiment, thus the impact of sweat on the sensing performance is still unknown. In the future, we will test our prototypes with users performing vigorous exercises to examine the system performance under excessive sweating. We will explore thinner fabrics to help the body better dissipate heat. Also, we will consider arranging insulative layers close to skin to protect sensing fabrics and the few conductive threads connecting to the micro-controller from sweat.
- From experiments we noticed that when the sensing fabric is not well fitting the joint surface, joint motion occasionally wrinkles the fabric, which affects fabric resistance and causes larger errors in inferring joint angles. This issue is partially due to limited (two) size options of current prototypes, which do not fit well for some participants. We plan to fabricate prototypes in more sizes to ensure exact tightness and reduce wrinkles. We will also consider designing prototypes with adjustable sizes using the nylon fastener tape. Additionally, we will explore fabrics with better elasticity so that they can retract/stretch more quickly to better fit joint surface during fast motion.
- Our current evaluation is based on a relative small user population and using environment. For more thorough evaluations, we plan to recruit more participants to test out our prototypes for tracking joint motion in diverse activities (e.g., practicing yoga poses, playing tennis). We will conduct long-term studies to examine the durability of the system (especially after repeated washes). We are also reaching out to orthopedists at a local hospital and discuss possible uses of our prototypes in medical applications. Also, we will test the prototype with participants pressing the joint against other objects.

REFERENCES

[1] 2018. Compression Arm Sleeve. https://www.amazon.com/d/Elbow-Braces/Kunto-Fitness-Compression-Tendonitis-Treatment/B010P9Q13K/ref=sr_1_1_sspa?s=sporting-goods&ie=UTF8&qid=1542318962&sr=1-1-spons&keywords=Compression+Arm+Sleeve&psc=1
[2] 2018. Compression Sleeve. https://www.amazon.com/McDavid-Compression-Protection-Basketball-Baseball/dp/B016WZG6KO?ref_=Oct_BSellerC_9590773011_4&pf_rd_p=329f6528-119f-5272-a932-88cab21c7435&pf_rd_s=merchandised-search-6&pf_rd_t=101&pf_rd_i=9590773011&pf_rd_m=ATVPDKIKX0DER&pf_rd_r=39BDF952GDARHYTKSK6H&pf_rd_r=39BDF952GDARHYTKSK6H&pf_rd_p=329f6528-119f-5272-a932-88cab21c7435
[3] 2018. E-Skin Sensor. https://xenoma.com/eskin-dk
[4] 2018. Figur 8 Sensors. https://figur8tech.com/pages/research-and-development-kit
[5] 2018. Figur8 Tech. https://figur8tech.com/blogs/figur8
[6] 2018. Jacquard. https://atap.google.com/jacquard/

[7] 2018. Jacquard Commuter Trucker Jacket. https://www.theguardian.com/technology/2017/sep/26/jacquard-google-levis-smart-jacket-denim

[8] 2018. Jacquard Commuter Trucker Jacket (Showcase). https://www.youtube.com/watch?v=yJ-lcdMfziw

[9] 2018. Jacquard Materials: Thread. https://atap.google.com/jacquard/about/

[10] 2018. Jacquard Turns Your Clothes into Wearables. https://www.techrepublic.com/article/how-googles-project-jacquard-turns-your-clothes-into-wearables/

[11] 2018. Stretch Sense. https://www.stretchsense.com/stretch-sensors/

[12] 2018. Stretch Sense Circuit. https://www.stretchsense.com/smart-garments/

[13] 2018. Vicon. https://www.vicon.com/

[14] 2018. Xenoma E-Skin. https://xenoma.com/

[15] Amazon. 2018. Kinesiology Tape. https://www.amazon.com/KT-Tape-Kinesiology-Therapeutic-Sports/dp/B003DV9JGO/ref=sr_1_1/136-0678870-8281028?s=sports-and-fitness&ie=UTF8&qid=1533589584&sr=1-1&refinements=p_4%3AKT+Tape

[16] Ozgur Atalay, William Richard Kennon, and Erhan Demirok. 2015. Weft-Knitted Strain Sensor for Monitoring Respiratory Rate and Its Electro-Mechanical Modeling. *IEEE Sensors …* 15, 1 (2015), 110–122.

[17] S H Bae, Y Lee, B K Sharma, H J Lee, J H Kim, and J H Ahn. 2013. Graphene-based transparent strain sensor. *Carbon* 51 (2013), 236–242.

[18] Abdelkareem Bedri, Richard Li, Malcolm Haynes, Raj Prateek Kosaraju, Ishaan Grover, Temiloluwa Prioleau, Min Yan Beh, Mayank Goel, Thad Starner, and Gregory Abowd. 2017. EarBit: Using Wearable Sensors to Detect Eating Episodes in Unconstrained Environments. *Proceedings of the ACM on Interactive, Mobile, Wearable and Ubiquitous Technologies* 1, 3 (Sept. 2017), 37–20.

[19] Mary Ellen Berglund, Julia Duvall, and Lucy E Dunne. 2016. A survey of the historical scope and current trends of wearable technology applications. *ISWC* (2016), 40–43.

[20] Ceren Günenç Beşer, Deniz Demiryürek, Hakan Özsoy, Burcu Erçakmak, Mutlu Hayran, Onur Kızılay, and Arzu Özsoy. 2014. Redefining the proximal ulna anatomy. *Surgical and Radiologic Anatomy* 36, 10 (July 2014), 1023–1031.

[21] T Bhattacharjee, A Jain, S Vaish, M D Killpack, and C C Kemp. 2013. Tactile sensing over articulated joints with stretchable sensors. In *2013 World Haptics Conference (WHC 2013)*. IEEE, 103–108.

[22] Johann Borenstein, Lauro Ojeda, and Surat Kwanmuang. 2009. Heuristic reduction of gyro drift in IMU-based personnel tracking systems. In *SPIE Defense, Security, and Sensing*, Craig S Halvorson, Šárka O Southern, B V K Vijaya Kumar, Salil Prabhakar, and Arun A Ross (Eds.). SPIE, 73061H.

[23] Toni E Campbell, Bridget J Munro, Gordon G Wallace, and Julie R Steele. 2007. Can fabric sensors monitor breast motion? *Journal of Biomechanics* 40, 13 (2007), 3056–3059.

[24] Matthieu K Chardon, Yasin Y Dhaher, Nina I Suresh, Giselle Jaramillo, and W Zev Rymer. 2015. Estimation of musculotendon kinematics under controlled tendon indentation. *Journal of Biomechanics* 48, 13 (Oct. 2015), 3568–3576.

[25] A. Derungs, S. Soller, A. WeishÃďupl, J. Bleuel, G. Berschin, and O. Amft. 2018. Regression-based, mistake-driven movement skill estimation in Nordic Walking using wearable inertial sensors. In *2018 IEEE International Conference on Pervasive Computing and Communications (PerCom)*. 1–10. https://doi.org/10.1109/PERCOM.2018.8444576

[26] M. Donno, E. Palange, F. Di Nicola, G. Bucci, and F. Ciancetta. 2008. A New Flexible Optical Fiber Goniometer for Dynamic Angular Measurements: Application to Human Joint Movement Monitoring. *IEEE Transactions on Instrumentation and Measurement* 57, 8 (Aug 2008), 1614–1620. https://doi.org/10.1109/TIM.2008.925336

[27] Tsutomu Fujimura. 2012. Investigation of the relationship between wrinkle formation and deformation of the skin using three-dimensional motion analysis. *Skin Research and Technology* 19, 1 (June 2012), e318–e324.

[28] Shin-ichi Fujiwara, Hajime Taru, and Daisuke Suzuki. 2010. Shape of articular surface of crocodilian (Archosauria) elbow joints and its relevance to sauropsids. *Journal of Morphology* 1 (2010), NA–NA.

[29] Peter T. Gibbs and HHarry Asada. 2005. Wearable Conductive Fiber Sensors for Multi-Axis Human Joint Angle Measurements. *Journal of NeuroEngineering and Rehabilitation* 2, 1 (02 Mar 2005), 7. https://doi.org/10.1186/1743-0003-2-7

[30] Guido Gioberto and Lucy E Dunne. 2012. Garment Positioning and Drift in Garment-Integrated Wearable Sensing. In *2012 16th Annual International Symposium on Wearable Computers (ISWC)*. IEEE, 64–71.

[31] R. Gnanadesikan. 1977. *Methods for statistical data analysis of multivariate observations / R. Gnanadesikan.* Wiley New York. x, 311 p. : pages.

[32] Linsey Griffin, Crystal Compton, and Lucy E Dunne. 2016. An analysis of the variability of anatomical body references within ready-to-wear garment sizes. In *Proceedings of the 2016 ACM International Symposium on Wearable Computers - ISWC '16*.

[33] H Harms, O Amft, and D Roggen. 2009. Rapid prototyping of smart garments for activity-aware applications. *Journal of Ambient …* (2009).

[34] Ragnar Holm. 1967. Electric Contacts. Springer Berlin Heidelberg, Berlin, Heidelberg.

[35] Ragnar Holm. 2013. *Electric contacts: theory and application.* Springer Science & Business Media.

[36] https://academic.csuohio.edu/. 2018. Linear Viscoelasticity. https://academic.csuohio.edu/duffy_s/Linear_Visco.pdf

[37] LessEMF Inc. 2018. Stretch Conductive Fabric. Retrieved Aug 4, 2018 from https://www.lessemf.com/321.pdf

[38] Joaan. 2018. Superflex Performance Fabric. https://www.joann.com/superflex-compression-performance-fabric-black/15226897.html#q=performance%2Bfabric&prefn1=prod_type&sz=36&start=37&prefv1=Product

[39] Joann.com. 2018. Micro-Flex Knit Fabric. Retrieved Aug 10, 2018 from https://www.joann.com/loungeletics-performance-micro-flex-compression-knit-fabric-59-heather/15781511.html

[40] Ali Kiaghadi, Morgan Baima, Jeremy Gummeson, Trisha Andrew, and Deepak Ganesan. 2018. Fabric as a Sensor: Towards Unobtrusive Sensing of Human Behavior with Triboelectric Textiles. In *Proceedings of the 16th ACM Conference on Embedded Networked Sensor Systems, SenSys 2018, Shenzhen, China, November 4-7, 2018*. 199–210. https://doi.org/10.1145/3274783.3274845

[41] Laurel Kuxhaus, Sisi Zeng, and Charles J Robinson. 2014. Dependence of elbow joint stiffness measurements on speed, angle, and muscle contraction level. *Journal of Biomechanics* 47, 5 (March 2014), 1234–1237.

[42] Yordan Kyosev. 2018. Narrow and Smart Textiles. Springer International Publishing, Cham.

[43] S Laksanacharoen and S Wongsiri. [n. d.]. Design of apparatus to study human elbow joint motion. In *IEEE EMBS Asian-Pacific Conference on Biomedical Engineering, 2003.* IEEE, 236–237.

[44] Alberto Leardini, Lorenzo Chiari, Ugo Della Croce, and Aurelio Cappozzo. 2005. Human movement analysis using stereophotogrammetry. *Gait & Posture* 21, 2 (Feb. 2005), 212–225.

[45] Jaehong Lee, Hyukho Kwon, Jungmok Seo, Sera Shin, Ja Hoon Koo, Changhyun Pang, Seungbae Son, Jae Hyung Kim, Yong Hoon Jang, Dae Eun Kim, and Taeyoon Lee. 2015. Conductive Fiber-Based Ultrasensitive Textile Pressure Sensor for Wearable Electronics. 27, 15 (2015), 2433–2439.

[46] S. I. Lee, J. Daneault, L. Weydert, and P. Bonato. 2016. A novel flexible wearable sensor for estimating joint-angles. In *2016 IEEE 13th International Conference on Wearable and Implantable Body Sensor Networks (BSN)*. 377–382. https://doi.org/10.1109/BSN.2016.7516291

[47] G Ligorio, D Zanotto, A M Sabatini, and S K Agrawal. 2017. A novel functional calibration method for real-time elbow joint angles estimation with magnetic-inertial sensors. *Journal of Biomechanics* 54 (March 2017), 106–110.

[48] Xiaoyou Lin and Boon-Chong Seet. 2015. A Linear Wide-Range Textile Pressure Sensor Integrally Embedded in Regular Fabric. 15, 10 (Aug. 2015), 5384–5385.

[49] F Lorussi, E P Scilingo, A Tesconi, A Tognetti, and D De Rossi. [n. d.]. Wearable sensing garment for posture detection, rehabilitation and tele-medicine. In *International Conference on Information Technology - Applications in Biomedicine*. IEEE, 287–290.

[50] Corinne Mattmann, Oliver Amft, Holger Harms, Gerhard Tröster, and Frank Clemens. 2007. Recognizing Upper Body Postures using Textile Strain Sensors. *ISWC* (2007), 1–8.

[51] Y Mengüç and Y L Park. 2013. Soft wearable motion sensing suit for lower limb biomechanics measurements. … *(ICRA)* (2013).

[52] Pierre Merriaux, Yohan Dupuis, RÃľmi Boutteau, Pascal Vasseur, and Xavier Savatier. 2017. A Study of Vicon System Positioning Performance. *Sensors* 17, 7 (2017). https://doi.org/10.3390/s17071591

[53] Sebastian Münzner, Philip Schmidt, Attila Reiss, Michael Hanselmann, Rainer Stiefelhagen, and Robert Dürichen. 2017. CNN-based sensor fusion techniques for multimodal human activity recognition. *ISWC* (2017).

[54] W M Murray, S L Delp, TS Buchanan Journal of biomechanics, and 1995. [n. d.]. Variation of muscle moment arms with elbow and forearm position. *jbiomech.com* ([n. d.]).

[55] Michiro Negishi, Mark Abildgaard, Ilan Laufer, Terry Nixon, and Robert Todd Constable. 2008. An EEG (electroencephalogram) recording system with carbon wire electrodes for simultaneous EEG-fMRI (functional magnetic resonance imaging) recording. *Journal of Neuroscience Methods* 173, 1 (Aug. 2008), 99–107.

[56] N Obaid, M T Kortschot, M Sain Materials, and 2017. [n. d.]. Understanding the stress relaxation behavior of polymers reinforced with short elastic fibers. *mdpi.com* ([n. d.]).

[57] Kyung Wha Oh, Hyun Jin Park, and Seong Hun Kim. 2003. Stretchable conductive fabric for electrotherapy. *Journal of Applied Polymer Science* 88, 5 (May 2003), 1225–1229.

[58] Patrick Parzer, Adwait Sharma, Anita Vogl, Jürgen Steimle, Alex Olwal, and Michael Haller. 2017. SmartSleeve - Real-time Sensing of Surface and Deformation Gestures on Flexible, Interactive Textiles, using a Hybrid Gesture Detection Pipeline. *UIST* (2017), 565–577.

[59] Zhi-Tao Rao, Feng Yuan, Bing Li, and Ning Ma. 2014. Effect of elbow flexion angles on stress distribution of the proximal ulnar and radius bones under a vertical load: measurement using resistance strain gauges. *Journal of Orthopaedic Surgery and Research* 9, 1 (July 2014), 1–7.

[60] Jung-Sim Roh, Yotam Mann, Adrian Freed, and David Wessel. 2011. Robust and Reliable Fabric, Piezoresistive Multitouch Sensing Surfaces for Musical Controllers. *NIME* (2011).

[61] O Röhrle, M Sprenger, and S Schmitt. 2016. A two-muscle, continuum-mechanical forward simulation of the upper limb. *Biomechanics and Modeling in Mechanobiology* 16, 3 (Nov. 2016), 743–762.

[62] Stefan Schneegass and Alexandra Voit. 2016. GestureSleeve - using touch sensitive fabrics for gestural input on the forearm for controlling smartwatches. *ISWC* (2016).

[63] M Sergio, N Manaresi, F Campi, R Canegallo, M Tartagni, and R Guerrieri. 2003. A dynamically reconfigurable monolithic cmos pressure sensor for smart fabric. *IEEE Journal of Solid-State Circuits* 38, 6 (June 2003), 966–975.

[64] Shayan Seyedin, Joselito M Razal, Peter C Innis, Ali Jeiranikhameneh, Stephen Beirne, and Gordon G Wallace. 2015. Knitted Strain Sensor Textiles of Highly Conductive All-Polymeric Fibers. *ACS Applied Materials & Interfaces* 7, 38 (Sept. 2015), 21150–21158.
[65] Tien-Wei Shyr, Jing-Wen Shie, Chang-Han Jiang, and Jung-Jen Li. 2014. A Textile-Based Wearable Sensing Device Designed for Monitoring the Flexion Angle of Elbow and Knee Movements. *Sensors* 14, 3 (March 2014), 4050–4059.
[66] Hloniphile M Sithole, Sabyasachi Mondal, Precious Sibanda, and Sandile S Motsa. 2017. An unsteady MHD Maxwell nanofluid flow with convective boundary conditions using spectral local linearization method. *Open Physics* 15, 1 (Oct. 2017), 637–646.
[67] S Šlajpah, R Kamnik, and M Munih. 2014. Kinematics based sensory fusion for wearable motion assessment in human walking. *Computer Methods and Programs in Biomedicine* 116, 2 (Sept. 2014), 131–144.
[68] sorbothane.com. 2018. Hinge Joint. http://www.innerbody.com/image_skel07/skel31.html
[69] sparkfun. 2018. NW170-PI-20. PDF. https://cdn.sparkfun.com/datasheets/E-Textiles/Materials/NW170-PI-20%20TDS.pdf
[70] sparkfun. 2018. NW170-SLPA-2k. PDF. https://cdn.sparkfun.com/datasheets/E-Textiles/Materials/NW170-SLPA-2k%20TDS.pdf
[71] sparkfun. 2018. Velostat. PDF. https://cdn.sparkfun.com/datasheets/E-Textiles/Materials/NW170-PI-20%20TDS.pdf
[72] Seiichi Takamatsu, Takahiro Yamashita, and Toshihiro Itoh. 2016. Meter-scale large-area capacitive pressure sensors with fabric with stripe electrodes of conductive polymer-coated fibers. *Microsystem Technologies* 22, 3 (Feb. 2016), 451–457.
[73] Xiaoming Tao. 2005. Wearable eletronics and photonics. Elsevier.
[74] Alessandro Tognetti, Federico Lorussi, Nicola Carbonaro, and Danilo de Rossi. 2015. Wearable Goniometer and Accelerometer Sensory Fusion for Knee Joint Angle Measurement in Daily Life. *Sensors* 15, 11 (Nov. 2015), 28435–28455.
[75] Takanori Uchiyama, Tomoyuki Bessho, and Kenzo Akazawa. 1998. Static torque–angle relation of human elbow joint estimated with artificial neural network technique. *Journal of Biomechanics* 31, 6 (1998), 545–554.
[76] E J Van Zuylen, A van Velzen, and J J Denier van der Gon. 1988. A biomechanical model for flexion torques of human arm muscles as a function of elbow angle. *Journal of Biomechanics* 21, 3 (Jan. 1988), 183–190.
[77] Anita Vogl, Patrick Parzer, Teo Babic, Joanne Leong, Alex Olwal, and Michael Haller. 2017. StretchEBand - Enabling Fabric-based Interactions through Rapid Fabrication of Textile Stretch Sensors. *CHI* (2017).
[78] Sylvie Charlotte Frieda Anneliese von Werder and Catherine Disselhorst-Klug. 2016. The role of biceps brachii and brachioradialis for the control of elbow flexion and extension movements. *Journal of Electromyography and Kinesiology* 28, C (June 2016), 67–75.
[79] Junpu Wang, Pu Xue, Xiaoming Tao, and Tongxi Yu. 2013. Strain Sensing Behavior and Its Mechanisms of Electrically Conductive PPy-Coated Fabric. *Advanced Engineering Materials* 16, 5 (2013), 565–570.
[80] Zehong Wang, Wei Wang, and Dan Yu. 2017. Pressure responsive PET fabrics via constructing conductive wrinkles at room temperature. *Chemical Engineering Journal* 330 (Dec. 2017), 146–156.
[81] I Wicaksono. 2016. Design and Implementation of Multi-sensory Fabric as Deformable Musical Interface. (2016).
[82] Wikipedia. 2018. Gaussian Kernel Smoother. https://en.wikipedia.org/wiki/Kernel_smoother
[83] Wikipedia. 2018. Local Regression. https://en.wikipedia.org/wiki/Local_regression
[84] Wikipedia. 2018. SavitzkyâĂŞGolay filter. https://en.wikipedia.org/wiki/Savitzky%E2%80%93Golay_filter
[85] Wikipedia. 2018. Standard Linear Solid Model. https://en.wikipedia.org/wiki/Standard_linear_solid_model#Kelvin_representation
[86] M. B. Wilk and R. Gnanadesikan. 1968. Probability Plotting Methods for the Analysis of Data. *Biometrika* 55, 1 (1968), 1–17. http://www.jstor.org/stable/2334448
[87] www.nurbsfactor.com. 2018. Vicon Camera. http://www.nurbsfactor.com/hardware_vicon.php
[88] A Yao and M Soleimani. 2012. A pressure mapping imaging device based on electrical impedance tomography of conductive fabrics. 32, 4 (Sept. 2012), 310–317.
[89] Hui Zhang, Xiaoming Tao, Shanyuan Wang, and Tongxi Yu. 2016. Electro-Mechanical Properties of Knitted Fabric Made From Conductive Multi-Filament Yarn Under Unidirectional Extension. *Textile Research Journal* 75, 8 (July 2016), 598–606.
[90] Wu Zhou, Peng Peng, Huijun Yu, Bei Peng, and Xiaoping He. 2017. Material Viscoelasticity-Induced Drift of Micro-Accelerometers. *Materials* 10, 9 (2017), 1077.
[91] R Zhu and Z Zhou. 2004. A Real-Time Articulated Human Motion Tracking Using Tri-Axis Inertial/Magnetic Sensors Package. *IEEE Transactions on Neural Systems and Rehabilitation Engineering* 12, 2 (June 2004), 295–302.
[92] Matthias A Zumstein, Alexander Bürki, Anne-Sophie Massy, Philippe Zysset, and Beat K Moor. 2015. Extra-articular step osteotomy of the olecranon: A biomechanical assessment. *Clinical Biomechanics* 30, 10 (Dec. 2015), 1043–1048.